Ab Initio Study of Structural and Magnetic Properties of TMn(ferrocene)n+1 (TM = Sc, Ti, V, Mn) Sandwich Clusters and Nanowires (n = ∞)

4 AUTHORS, INCLUDING:

Xiuyun Zhang
Yangzhou University
25 PUBLICATIONS **410** CITATIONS

Yi Gao
Shanghai Institute of Applied Physics
81 PUBLICATIONS **1,795** CITATIONS

Zeng Cheng
University of Science and Technology of C…
379 PUBLICATIONS **6,788** CITATIONS

Ab Initio Study of Structural and Magnetic Properties of TM$_n$(ferrocene)$_{n+1}$ (TM = Sc, Ti, V, Mn) Sandwich Clusters and Nanowires ($n = \infty$)

Xiuyun Zhang,[†] Jinlan Wang,[†,]* Yi Gao,[‡] and Xiao Cheng Zeng[‡,]*

[†]Department of Physics, Southeast University, Nanjing, 211189, P.R. China, and [‡]Department of Chemistry and Nebraska Center for Materials and Nanoscience, University of Nebraska, Lincoln, Nebraska 68588

Since the discovery of ferrocene [Fe(C$_5$H$_5$)$_2$] in 1951,[1] studies of metal−organic-molecule complexes have been an active area of research in organometallic chemistry. These complexes have found applications, among others, in catalysis, molecular recognition, and nanomagnetism.[2] Especially, multidecker sandwich complexes have attracted considerable attention because of their intriguing structural, magnetic, and transport properties.[2−35] For example, previous experimental and theoretical studies have shown that multidecker sandwich forms are the most stable for Sc−, Ti−, and V−C$_6$H$_6$ (Bz) complexes,[3−21] as well as for the lanthanide rare earth metal−C$_8$H$_8$ complexes.[22−30] Experimentally, seven-decker V$_n$(Bz)$_m$ sandwich clusters and eighteen-decker Eu$_n$(C$_8$H$_8$)$_m$ nanorods have been synthesized by means of a laser vaporization synthesis technique.[30] Theoretically, Wang *et al.*[12] identified a structural transition from achiral D_{6h} to chiral D_2 structure for the V$_4$Bz$_5$ sandwich cluster. Such a structural transition can be verified from either broadened IR spectra or appearance of new IR modes in an infrared (IR) spectroscopy experiment.[13]

There are also growing interests in magnetic properties of multidecker sandwich complexes. Miyajima *et al.*[8] detected monotonic increase of the magnetic moment with cluster size n for V$_n$(Bz)$_{n+1}$ ($n = 1-4$) and Sc$_n$(Bz)$_{n+1}$ ($n = 1-2$), as well as nonzero magnetic moments for Ti$_n$Bz$_{n+1}$ ($n = 2, 3$) in their Stern−Gerlach molecular beam deflection experiment. They also detected

high magnetic moments in Ln$_n$(C$_8$H$_8$)$_m$ ($n = 1-7$, $m = n - 1$, n, $n + 1$, Ln = Eu, Tb, Ho, Tm) clusters.[25,26] Theoretical studies by Kandalam *et al.*[11] showed that the magnetic moment of V$_n$(Bz)$_{n+1}$ increases linearly with size n, and V atoms are coupled ferromagnetically. Wang *et al.*[12] suggested that the measured magnetic moments of V$_n$(Bz)$_{n+1}$ can be considered as an average over different spin states of low-lying isomers. However, Weng *et al.*[21] found that ferromagnetic state of V$_2$Bz$_3$ is unstable.

Besides finite-size clusters, infinitely long sandwich complexes (or nanowires) [TMBz]$_\infty$ (TM = transition metal) also exhibit novel magnetic and transport properties.[16−21] Xiang *et al.*[17] revealed from their density-functional theory calculations that Mn−Bz sandwich nanowire is a half-metallic ferromagnet and V−Bz is a quasi-half-metallic ferromagnet, but Ti−Bz is antiferromagnetic and Sc−Bz is paramagnetic. Conversely, Rahman *et al.*[16] and Maslyuk

ABSTRACT Structural and magnetic properties of multidecker sandwich clusters TM$_n$(ferrocene)$_{n+1}$ [TM = V, Ti, Sc, Mn, ferrocene=FeCp$_2$, $n = 1-3$] and corresponding one-dimensional sandwich nanowires ($n = \infty$) are studied by means of gradient-corrected density functional theory. The TM$_n$(FeCp$_2$)$_{n+1}$ clusters are highly stable polyferrocene-like sandwich structures due to strong Fe−Cp interaction. The total magnetic moment of TM$_n$(FeCp$_2$)$_{n+1}$ (TM = V, Ti, Mn) increases linearly with the size n. More strikingly, Ti$_n$(FeCp$_2$)$_{n+1}$ and V$_n$(FeCp$_2$)$_{n+1}$ ($n = 1-3$) exhibit high magnetic moments 4, 8, 12 μ_B and 1, 6, 11 μ_B, respectively. In contrast, Sc$_n$(FeCp$_2$)$_{n+1}$ clusters are paramagnetic. The [TM(FeCp$_2$)]$_\infty$ sandwich nanowires are ferromagnetic semiconductors whose band gap is 0.361, 0.506, 0.51, and 1.310 eV, respectively, for TM = Ti, Sc, V, and Mn. Among the four sandwich nanowires, [V(FeCp$_2$)]$_\infty$ nanowire possesses the highest magnetic moment (5 μ_B) per unit cell.

KEYWORDS: sandwich clusters and nanowires · density functional theory · high magnetic moments · nanomagnetism
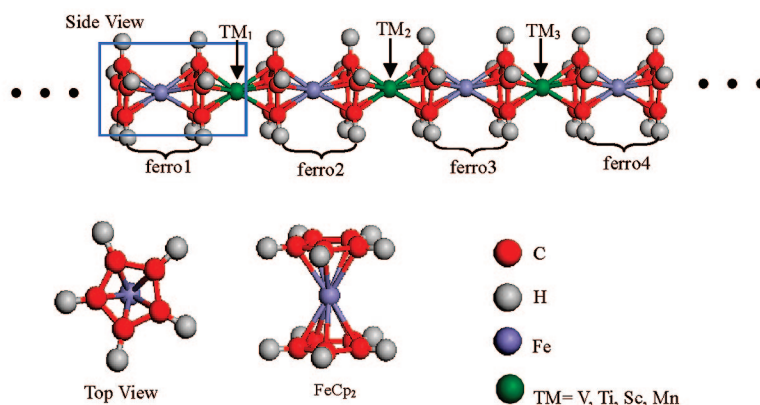
© 2009 American Chemical Society

Multidecker sandwich clusters

Figure 1. Sketches of $TM_n(FeCp_2)_{n+1}$ (up to $n = 3$) multidecker sandwich cluster and 1D infinitely long $[TM(FeCp_2)]_\infty$ sandwich nanowire.

et al.[18] both predicted that V−Bz sandwich nanowire is a half-metallic ferromagnet. Maslyuk et al.[18] further suggested that the V−Bz sandwich nanowire can be potentially a spin filter. Koleini et al.[34] proposed an efficient organometallic spin filter by placing V_nBz_m clusters between two single-wall carbon nanotube (or graphene) electrodes. They found high transmission spin polarization from 73% (strong bonds) up to 99% (weak bonds), independent of specific structure or orientation of V_nBz_m. Atodiresei et al.[35] also found that magnetization direction in organic magnetic molecules can be altered by controlling their oxidation state. For example, a change of magnetization direction, from in-plane to axial, can be observed by charging or discharging $Eu_2(C_8H_8)_3$ molecule.

Despite many ferrocene-like molecules such as VCp_2, $CrCp_2$, $MnCp_2$, $CoCp_2$, $NiCp_2$, and $ZnCp_2$ being synthesized experimentally[36−45] or studied theoretically,[46−57] only a few studies were reported on the multidecker

sandwich clusters based on the C_5H_5 ligands. Triple-decker sandwich complexes $Ni_2Cp_3^+$ and $Fe_2Cp_3^+$ were synthesized in the 70s.[58,59] Later, Nagao et al.[60] synthesized multidecker sandwich complexes $TM_n(FeCp_2)_{n+1}$ (TM = V, Ti, $n = 1-3$). Theoretically, Zhou et al.[31] and Shen et al.[32] studied ferromagnetic properties of first-raw transition metal−Cp (Cp = C_5H_5) sandwich nanowires. Wang et al.[33] investigated magnetic properties of $V_n(FeCp_2)_{n+1}$ clusters and nanowire. In this paper, we present a systematic *ab initio* study of structural and magnetic properties of multidecker sandwich clusters $TM_n(FeCp_2)_{n+1}$ (TM = Sc, Ti, V, Mn, $n = 1-3$), as well as the corresponding one-dimensional (1D) [TM-(FeCp_2)]_∞ sandwich nanowires. We find that $TM_n(FeCp_2)_{n+1}$ (TM = V, Ti, Mn) clusters are ferromagnetic and their magnetic moment increases linearly with n. In contrast, the $Sc_n(FeCp_2)_{n+1}$ clusters are paramagnetic. The four sandwich nanowires $[TM(FeCp_2)]_\infty$ are all ferromagnetic semiconductors with band gap ranging from 0.361 to 1.310 eV. The V-, Ti- and Mn-nanowires exhibit high magnetic moment of 5, 4, and 3 μ_B per unit cell, respectively.

RESULTS AND DISCUSSION

Multidecker Sandwich Clusters. *Structural Properties.* Geometric sketches of multidecker sandwich clusters $TM_n(FeCp_2)_{n+1}$ and 1D $[TM(FeCp_2)]_\infty$ nanowires are shown in Figure 1. Lowest-energy structures of these clusters are presented in Figure S1 in the Supporting Information. The size-specified structural, energetic, electronic, and magnetic properties of the lowest-energy clusters $TM_n(FeCp_2)_{n+1}$ (TM = Ti, Sc, V, Mn) are summarized in Table 1. Only $Mn_2(FeCp_2)_3$, $Ti_2(FeCp_2)_3$, and $Ti_3(FeCp_2)_4$ have D_{5h} symmetry, and all other $TM_n(FeCp_2)_{n+1}$ clusters have lower symmetries than D_{5h}. Vibrational frequency analysis shows that D_{5h}-$TM(FeCp_2)_2$ (TM = V, Ti, and Mn) and D_{5h}-$Mn_3(FeCp_2)_4$ clusters have imaginary frequencies and the stable structures of these clusters adopt a lower symmetry such as C_{2v}, C_2, or C_s. Moreover, imposing D_{5h} symmetry on $Sc(FeCp_2)_2$, $V_2(FeCp_2)_3$, $V_3(FeCp_2)_4$, and $Sc_3(FeCp_2)_4$ clusters results in exact (or near) degeneracy of the highest occupied molecular orbital (HOMO) and the lowest unoccupied molecular orbital (LUMO). Hence, the energetically preferred low-symmetry structure is a consequence of the Jahn−Teller effect, which gives rise to a finite HOMO−LUMO gap (0.295−0.717 eV) and lower energies (0.14−0.24 eV) for these clusters. As shown in Figure 2, exact degenerate orbitals (HOMO/LUMO, labeled as $e_{1'}$) for D_{5h}-$Sc_3(FeCp_2)_4$ are split into two close orbitals in the low-symmetry C_1 structure (both labeled as a), which may be the underlying reason for the distortion of $Sc_3(FeCp_2)_4$ cluster. The signifi-

TABLE 1. Point Group Symmetry (PGS), Magnetic Moment (M), Average Distance between TM and Cp Ligand (R_{TM-Cp}, R_{Fe-Cp}), HOMO−LUMO gap (Δ), Average Binding Energy BE_{FeCp_2} and BE, and Their Differences, $BE-BE_{FeCp_2}$, of the Lowest-Energy Structure of $FeCp_2$ and $TM_n(FeCp_2)_{n+1}$ ($n = 1-3$)

cluster	PGS	M (μ_B)	R_{TM-Cp} (Å)	R_{Fe-Cp} (Å)	Δ (eV)	BE_{FeCp_2} (eV)	BE (eV)	$BE-BE_{FeCp_2}$ (eV)
$FeCp_2$	D_{5h}	0		1.670	3.186		8.22	
$V_1(FeCp_2)_2$	C_2	1	1.847	1.702	0.747	2.021	6.150	4.129
$V_2(FeCp_2)_3$	C_{2v}	6	1.891	1.740	0.717	2.290	5.847	3.557
$V_3(FeCp_2)_4$	C_2	11	1.901	1.757	0.632	2.430	5.729	3.299
$Ti_1(FeCp_2)_2$	C_{2v}	4	2.034	1.701	0.184	2.191	6.210	4.019
$Ti_2(FeCp_2)_3^a$	D_{5h}	8	2.031	1.713	0.295	2.423	5.907	3.484
$Ti_3(FeCp_2)_4^a$	D_{5h}	12	2.030	1.725	0.469	2.583	5.804	3.211
$Sc_1(FeCp_2)_2$	C_1	1	2.100	1.715	0.532	2.084	6.175	4.091
$Sc_2(FeCp_2)_3$	C_1	0	2.093	1.725	0.669	2.300	5.852	3.552
$Sc_3(FeCp_2)_4$	C_1	1	2.080	1.820	0.545	2.369	5.712	3.343
$Mn_1(FeCp_2)_2$	C_s	1	1.697	1.699	0.302	1.064	5.834	4.770
$Mn_2(FeCp_2)_3$	D_{5h}	2	1.695	1.712	0.228	1.250	5.431	4.181
$Mn_3(FeCp_2)_4$	C_2	3	1.693	1.722	0.024	1.285	5.248	3.963

^{a}The optimized structures are obtained using a thermal smearing value of 0.005 au.

cant deformation of this cluster (see Figure S1 in the Supporting Information) may be correlated with the fact that Sc has fewer valence electrons $(3d^1 4s^2)$ and thus may have relatively weaker interaction with the $FeCp_2$ molecule than other TMs.

The C$-$H (R_{C-H}) bond length in $TM_n(FeCp_2)_{n+1}$ clusters is $\sim$1.086 Å, close to the value in isolated $FeCp_2$ molecule. The C$-$C bond length (R_{C-C}) varies, dependent on the location of Cp ring in the clusters: $R_{C-C} =$ 1.43 Å for the two side Cp rings, increases toward the center of the clusters, and reaches a maximum value of 1.508 Å for $Sc_2(FeCp_2)_3$. For the Fe$-$Cp distance R_{Fe-Cp}, at the two end of all clusters, it is close to that (1.670 Å) in the isolated ferrocene molecule, but increases toward the center of $TM_n(FeCp_2)_{n+1}$ clusters, with values ranging from 1.76 Å (for TM = Ti, V, and Mn) to 2.146 Å (for TM = Sc). The distance R_{TM-Cp} (TM $\neq$ Fe) is generally much longer than R_{Fe-Cp} for TM $=$Sc, Ti, and V, but comparable to R_{Fe-Cp} for TM = Mn (see Table 1). The different structural behavior can be seen more clearly in Figure S1, where all metal$-$ring distances are presented. Although R_{Mn-Cp} is much smaller than R_{TM-Cp} (TM = V, Ti, Sc), the variation ratios of R_{TM-Cp} for TM = V, Ti, Sc, and Mn are comparable, that is, R_{TM-Cp} are shortened by 1.5$\sim$4.9% compared to those in pure TM-Cp_2 complexes (1.942, 2.060, 2.145, and 1.769 Å for TM = V, Ti, Sc, and Mn, respectively).

Relative Stabilities. Relative stabilities of the clusters $TM_n(FeCp_2)_{n+1}$ are investigated on the basis of two forms of binding energies (BEs): (1) BE$(n) = \{nE[TM] + (n + 1)E[Fe] + 2(n + 1)E[Cp] - E[TM_n(FeCp_2)_{n+1}]\}/(2n + 1)$, and (2) $BE_{FeCp_2}(n) = \{nE[TM] + (n + 1)E[FeCp_2] - E[TM_n(FeCp_2)_{n+1}]\}/n$. The BE and BE_{FeCp2} measure the average metal$-$Cp and TM$-$FeCp$_2$ interaction, respectively. Here, $E[\cdot]$ denotes total energy of the cluster or atom. As shown in Table 1, BE_{FeCp_2} increases gradually with n for all clusters. For V$-$, Ti$-$, Sc$-$FeCp$_2$, $BE_{FeCp2} >$ 2.0 eV, but $BE_{FeCp_2} <$ 1.3 eV for Mn$-$FeCp$_2$. The latter behavior might be because the Mn atom is a stable half-filled electronic structure $(3d^5 4s^2)$ and thus has relatively high promotion energy from $4s^2 3d^5$ to $4s^1 3d^6$ and relatively weak bonding with the organic ligands.

On the other hand, BE decreases with n for all clusters, correlating with the trend of overall increased metal$-$ring distances $R_{TM-Cp} + R_{Fe-Cp}$ (Table 1). A similar trend has been found for V_nBz_{n+1} clusters ($n = 1-3$).[12] We suggest that the difference BE $-$ BE_{FeCp_2} may be used to characterize the Fe$-$Cp interaction. As shown in the last column of Table 1, some trends in BE $-$ BE_{FeCp2} can be seen: (1) BE $-$ BE_{FeCp2} decreases with increasing n, which correlates with the increased R_{Fe-Cp}. (2) Despite having the smallest BE and BE_{FeCp_2}, $Mn_n(FeCp_2)_{n+1}$ clusters actually show the greatest energy difference BE $-$ BE_{FeCp_2} and the shortest R_{Fe-Cp} among the four sandwich clusters. (3) BE $-$ BE_{FeCp_2} are much larger than BE_{FeCp_2} in all the four clusters, implying that the interaction between Fe and Cp is much

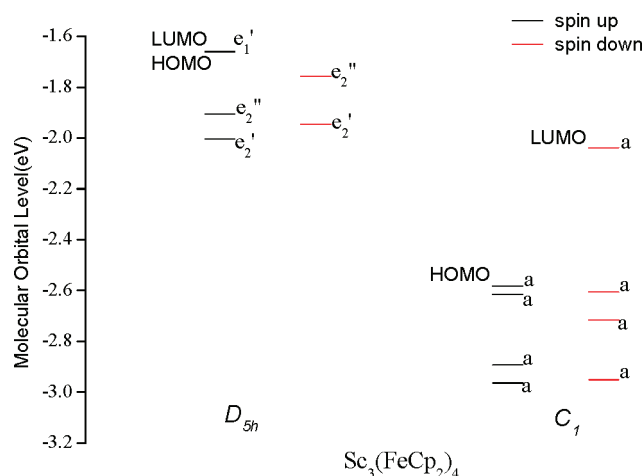**Figure 2. Frontier molecular orbitals of $Sc_3(FeCp_2)_4$ in high-symmetry D_{5h} and the lowest-energy C_1 structures.**

stronger than that of TM ($\neq$Fe)$-$Cp. This distinctive energy characteristic explains why all the clusters adopt "polyferrocene" sandwich-like structures as shown by experiments.[60]

Electronic and Magnetic Properties. The multidecker sandwich clusters exhibit different magnetic properties. All Ti$-$, V$-$, Mn$-$FeCp$_2$ clusters are ferromagnetic and their total magnetic moment increases linearly with n. More strikingly, $Ti_n(FeCp_2)_{n+1}$ and $V_n(FeCp_2)_{n+1}$ show large increment in the magnetic moment with increasing size n. The total magnetic moment of $Ti_n(FeCp_2)_{n+1}$ ($n = 1-3$) is 4, 8, 12 μ_B, respectively, and that of $V_n(FeCp_2)_{n+1}$ ($n = 1-3$) is 1, 6, 11 μ_B. The magnetic moment for $Mn_n(FeCp_2)_{n+1}$ is relatively small, which is 1, 2, 3 μ_B for $n = 1-3$. The stable spin state of $Sc_n(FeCp_2)_{n+1}$ is either a singlet with even-number electrons or a doublet with odd-number electrons, and thus $Sc_n(FeCp_2)_{n+1}$ is paramagnetic regardless of the size n. We should point out that Wang *et al.*[33] obtained higher magnetic moments of 5, 10, 15 μ_B for $V_n(FeCp_2)_{n+1}$ ($n = 1-3$). In our calculations, these spin states have close energies ($\Delta E =$0.018, 0.125, and 0.118 eV) with respect to the most stable spin states. This inconsistence may be due to different computational approaches and implemented codes (PW91/DNP in DMol *vs* norm-conserved pseudopotential PBE in Siesta). We also used PW91PW91/6-31G(d) level of theory implemented in the Gaussian 03 package[61] to verify these nearly degenerate spin states and found that the spin state of 5, 6, and 11 μ_B is 0.11, 0.023, and 0.028 eV lower in energy, respectively, than that of 1, 10, and 15 μ_B for $V_n(FeCp_2)_{n+1}$ ($n = 1-3$). Hence, multiple iso-energy isomers with different spins may coexist.

To understand differences in the magnetic properties of the TM (V, Ti, Mn, Sc)$-$FeCp$_2$ clusters, we show the occupied-frontier-orbital diagram and percentage contribution to d orbital from the TM and Fe atoms in Figure 3. Under D_{5h} structural symmetry of ligand field, the five degenerated d orbitals of Fe or TM are split
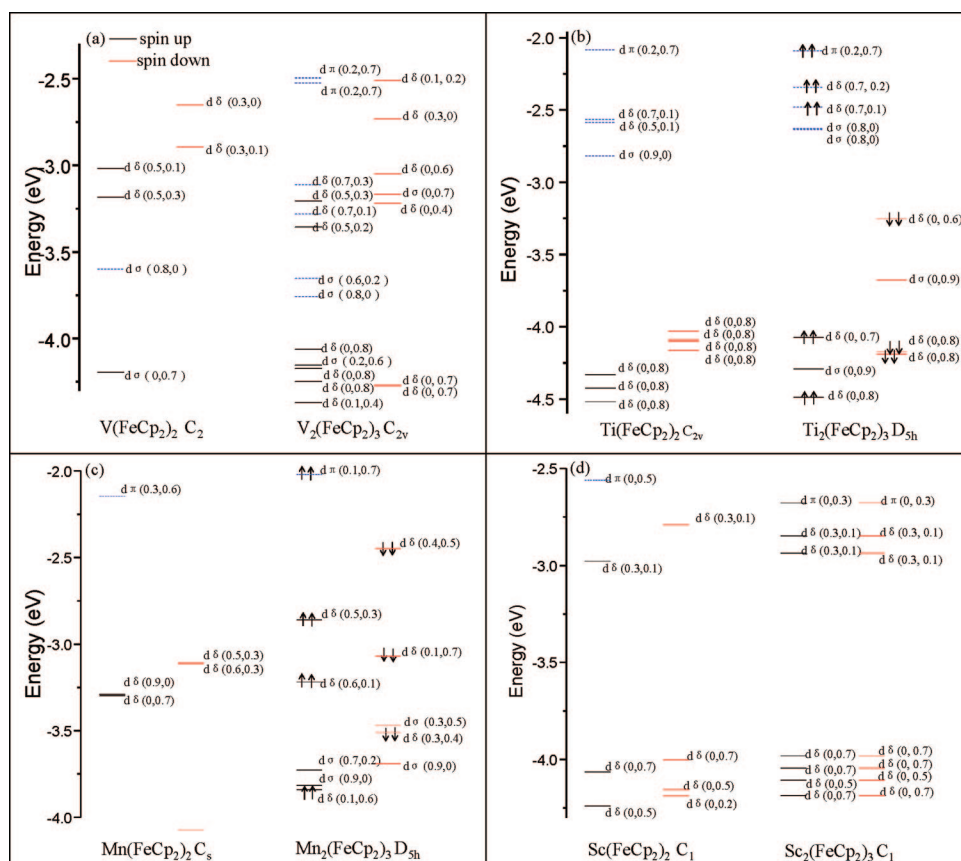
Figure 3. Occupied molecular orbitals diagrams of the lowest-energy structure of $TM_n(FeCp_2)_{n+1}$ (TM = V, Ti, Sc, Mn; n = 1,2) clusters. Blue dashed lines refer to orbitals responsible for the magnetic moment of the clusters. The two numbers in parenthesis are the percentage contribution from d orbitals of V (Ti, Sc, Mn) and Fe. The double arrows refer to those clusters with *doubly* degenerated spin-up (or spin-down) orbitals [*e.g.*, D_{5h}–$Ti_2(FeCp_2)_3$ and D_{5h}–$Mn_2(FeCp_2)_3$].

into one nondegenerate orbital σ (d_{z2} or a_1), two degenerate orbitals π (d_{yz}, d_{xz}, or e_1) and δ (d_{xy}, $d_{x^2-y^2}$, or e_2). These orbitals are fully split into five nondegenerate orbitals under structural symmetry of C_{2v} (or lower than C_{2v}) of ligand field. According to the Hückel rule ($4n$ + 2, where n is an integer), the Cp radical is short of one electron to form a stable aromatic structure. Therefore, a Cp ring tends to draw an extra electron from TM or Fe forming Cp^- in the cluster.[32]

In a ferrocene molecule, the Fe ($3d^6 4s^2$) atom behaves like Fe^{2+} with two electrons transferred to two neighboring Cp rings. For C_2-$V(FeCp_2)_2$, twelve d orbitals are contributed from Fe atoms, every Fe atom can transfer two valence electrons to its neighboring Cp rings as in pure ferrocene, and the two end $FeCp_2$ units contribute nearly zero magnetic moment to the cluster. On the other hand, the V atom possesses five valence d electrons (two 4s electrons fill the 3d shell in the metal−ligand clusters), three of them fill one σ(d_{z^2}) and two δ(d_{xy}, $d_{x^2-y^2}$) orbitals on the majority manifold and two of them fill two minority δ(d_{xy}, $d_{x^2-y^2}$) orbitals, ending up one unpaired electron to σ(d_{z^2}) orbital. Hence, the magnetic moment of $V(FeCp_2)_2$ is 1 μ_B. In C_{2v}-$V_2(FeCp_2)_3$, we identify eight d orbitals due mainly to the V atoms. Two σ(d_{z^2}) and four δ(d_{xy}, $d_{x^2-y^2}$) orbitals are filled in the majority channel and two δ(d_{xy},

$d_{x^2-y^2}$) orbitals are filled in the minority channel. As a result, two σ(d_{z^2}) and two δ(d_{xy}, $d_{x^2-y^2}$) majority electrons are unpaired and give rise to magnetic moment of 4 μ_B. Compared to $V(FeCp_2)_2$, one additional δ(d_{xy}, $d_{x^2-y^2}$) minority electron from every V atom is transferred to its neighboring Cp ring, which liberates two valence electrons of Fe atoms unpaired. This can be clearly seen from Figure 3a, two d electrons of the Fe atoms are pushed to the π(d_{yz}) orbitals in the majority channel, contributing a magnetic moment of 2 μ_B. Consequently, the total magnetic moment of C_{2v}-$V_2(FeCp_2)_3$ is 6 μ_B. Similar analysis can be carried out for $V_3(FeCp_2)_4$. Especially, the center V atom provides two electrons to its neighboring Cp rings, leaving three electrons on the majority manifold. As a result, the number of the unpaired electrons on V, Fe, V, Fe, V atoms is respectively 2, 2, 3, 2, 2, giving the total magnetic moment 11 μ_B for the sandwich cluster $V_3(FeCp_2)_4$.

Again, similar analysis can be performed for $TM_n(FeCp_2)_{n+1}$ (TM = Sc, Ti, and Mn). For C_{2v}-$Ti(FeCp_2)_2$, there are two δ (d_{xy}, $d_{x^2-y^2}$) and one σ (d_{z^2}) orbitals contributed mainly by the Ti atom on the majority channel. Hence, one d electron is transferred from Ti atom ($3d^2 4s^2$) to its adjacent Cp rings (two 4s electrons fill the 3d shell too, and the Ti atom thus has four d electrons in the cluster). As a result, one π(d_{yz}) electron of Fe

atoms is liberated on the majority channel. Overall, the Ti atom and two Fe atoms give rise to 3 μ_B and 1 μ_B magnetic moment, respectively, and the total magnetic moment is 4 μ_B. For D_{5h}-Ti$_2$(FeCp$_2$)$_3$, every Ti provides three unpaired d electrons to two δ(d$_{xy}$, d$_{x^2-y^2}$) and one σ(d$_{z^2}$) orbitals, the two outer Fe atoms jointly provide one unpaired electron to the π(d$_{yz}$) orbital, and the center Fe atom provides one unpaired electron to the π(d$_{yz}$) orbital. Overall, the total magnetic moment of Ti$_2$(FeCp$_2$)$_3$ cluster is 8 μ_B. In Figure 3b, we used up/down arrows to mark the doubly degenerated orbitals for D_{5h}-Ti$_2$(FeCp$_2$)$_3$. With the same reason, the total magnetic moment of Ti$_3$(FeCp$_2$)$_4$ cluster is 12 μ_B.

In the case of C_s-Mn(FeCp$_2$)$_2$, six d electrons from every Mn (3d^{5}4s^2) atom occupying the δ (d$_{xy}$, d$_{x^2-y^2}$) and σ (d$_{z^2}$) orbitals evenly on the majority and minority manifolds, suggesting that Mn transfers one electron to its adjacent Cp rings (Figure 3c). As a result, one electron liberated from Fe atoms occupies the π(d$_{yz}$) orbital unpaired, and the magnetic moment of Mn-(FeCp$_2$)$_2$ is 1 μ_B. Likewise, for C_1-Sc(FeCp$_2$)$_2$ (Figure 3d), the Sc atom transfers one valence electron to its adjacent Cp rings (the remaining two electrons occupied the dδ orbitals), and liberates one electron of Fe atom which contributes 1 μ_B magnetic moment. However, unlike Mn$_2$(FeCp$_2$)$_3$, the two liberated electrons of Fe atoms in the case of Sc$_2$(FeCp$_2$)$_3$ align pairedly, resulting in zero magnetic moment for Sc$_2$(FeCp$_2$)$_3$. We thus expect that Sc$_n$(FeCp$_2$)$_{n+1}$ clusters are paramagnetic and possess 1 μ_B magnetic moment when n is odd, and zero moment when n is even. Note that this electron transfer can explain the increase of Fe-Cp distance with size in all the four systems, as the cluster size n increases, more electrons transfer from TM (TM = V, Ti, Sc, Mn) atoms to the Cp rings, which lowers the oxidation states of Fe atoms and weakens the Fe−Cp interaction and thus increases the Fe−Cp distance.

1D [TM(FeCp$_2$)]$_\infty$ Sandwich Nanowires. Structural, binding energy and magnetic moments of 1D sandwich nanowires [TM-(FeCp$_2$)]$_\infty$ (TM = V, Ti, Sc, Mn) are summarized in Table 2. Structural features of the sandwich nanowires are similar to those of sandwich clusters. For example, [V(FeCp$_2$)]$_\infty$ nanowire has the largest unit-cell length c = 7.73 Å, while [Mn(FeCp$_2$)]$_\infty$ nanowire has the shortest length c = 7.22 Å. Moreover, R_{TM-Cp} is greater than R_{Fe-Cp} except TM = Mn. For the latter, R_{Mn-Cp} = 1.672 Å < R_{Fe-Cp} = 1.941Å.

The binding energy per unit cell of [TM-(FeCp$_2$)]$_\infty$ sandwich nanowire is defined as BE$_{FeCp2}$ = E(FeCp$_2$) + E(TM) − E[TM-(FeCp$_2$)]$_\infty$. Among the four types of nanowires, the [V(FeCp$_2$)]$_\infty$ nanowire has the largest BE$_{FeCp2}$ = 2.643 eV, followed by

TABLE 2. Unit-Cell Length (c), PGS, Bond Lengths, Binding Energy (BE$_{FeCp_2}$), Total Magnetic Moment Per Unit Cell (M), Band Gap (Gap), Energy Difference between FM and AFM (or PM) States [ΔE = E(FM) − E(AFM/PM)], and Electronic Ground State (GS) of 1D [TM(FeCp$_2$)]$_\infty$ (TM = V, Ti, Sc, Mn) Sandwich Nanowires

	V	Ti	Sc	Mn
c (Å)	7.46	7.50	7.73	7.22
PGS	C_{5v}	C_s	C_1	C_s
R_{C-C} (Å)	1.452, 1.453	1.447 − 1.464	1.445 − 1.512	1.450 − 1.463
R_{C-H} (Å)	1.085, 1.086	1.084, 1.085	1.084 − 1.090	1.085, 1.086
R_{Fe-Cp} (Å)	1.805, 1.804	1.735	1.681, 1.777	1.941
R_{TM-Cp} (Å)	1.924	2.016	2.210	1.672
BE$_{FeCp2}$ (eV)	2.643	2.625	2.377	1.466
M (μ_B)	5	4	1	3
gap	0.51	0.361	0.506	1.310
ΔE (eV)	0.77	0.48	0.11	0.32
GS	semiconductor	semiconductor	semiconductor	semiconductor

[Ti(FeCp$_2$)]$_\infty$ with BE$_{FeCp2}$ = 2.625 eV, and [Sc(FeCp$_2$)]$_\infty$ with BE$_{FeCp2}$ = 2.377 eV. As in the case of finite-size cluster Mn$_n$(FeCp$_2$)$_{n+1}$, [Mn(FeCp$_2$)]$_\infty$ has the least BE$_{FeCp2}$ = 1.466 eV.

Electronic structure calculations show that all four sandwich nanowires [TM(FeCp$_2$)]$_\infty$ (TM = V, Ti, Sc, Mn) exhibit sizable energy gaps, ranging from 0.361 to 1.310 eV (Table 2), indicating they are all semiconductors. Moreover, all the four sandwich nanowires are ferromagnetic with magnetic moment per unit cell being 5, 4, 1, and 3 μ_B, respectively, for TM = V, Ti, Sc, Mn. We have examined relative stability between the ferromagnetic state (FM) and antiferromagnetic (AFM) or paramagnetic (PM) state. The FM state is lower in energy (per unit cell) by 0.77, 0.48, 0.11, and 0.32 eV than the AFM or PM state, for TM = V, Ti, Sc, and Mn, respectively. In contrast, the 1D (V−Bz)$_\infty$ and (Mn−Bz)$_\infty$ sand-
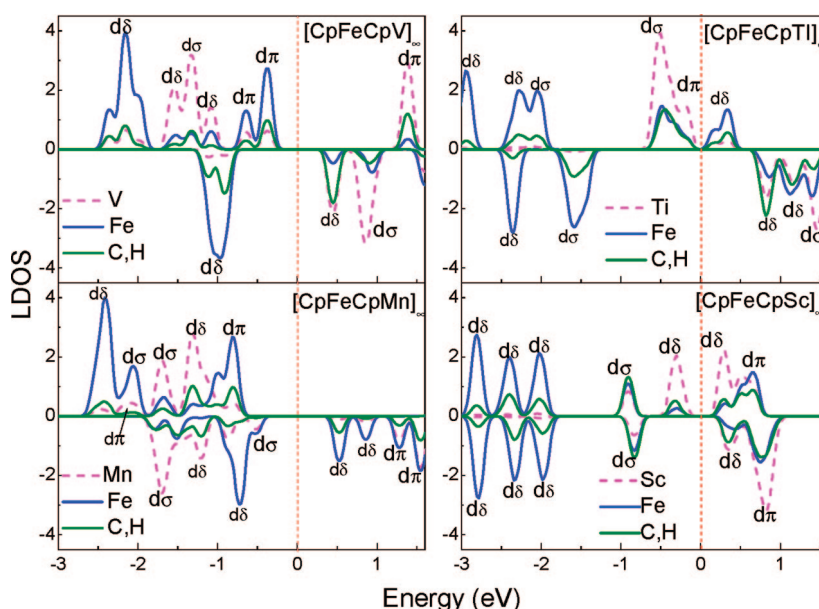
Figure 4. Local (LDOS) electronic density of state of 1D [TM(FeCp$_2$)]$_\infty$ nanowires and a ferrocene molecule. The dash line refers to shifted Fermi level which corresponds to (HOMO + LUMO)/2 here. Gaussian broadening of half-width 0.054 eV is used.

wich nanowires have smaller magnetic moment per unit cell (0.8 and 1.0 μ_B, respectively) than $[V(FeCp_2)]_\infty$ and $[Mn(FeCp_2)]_\infty$, while $(Sc-Bz)_\infty$ sandwich nanowire is paramagnetic and $(Ti-Bz)_\infty$ is AFM.[17] Hence, the replacement of benzene by ferrocene can significantly enhance ferromagnetic coupling within 1D sandwich nanowire.

In addition, some $[TM(FeCp_2)]_\infty$ sandwich nanowires may possess spin-polarized properties, similar to $[FeCp]_\infty$ and $[VCp]_\infty$ nanowires.[31,32] The latter two are actually half-metallic. For example, $[Ti(FeCp_2)]_\infty$ has a small gap of 0.361 eV in the majority channel and a large gap of 2.455 eV in the minority channel. If the small gap can be closed by applying an external electric field or an external mechanical force,[62] the sandwich nanowire may be turned into a half-metal as well.

Magnetism of the $[TM(FeCp_2)]_\infty$ sandwich nanowires can be understood from local density of states (LDOS) projected on TM, Fe, and Cp. As shown in Figure 4, for the V–, Ti–, and Mn–FeCp$_2$ nanowires, strong exchange splitting can be observed in d-projected LDOS of TM and Fe atoms. Near the Fermi level, the majority d electrons from TM atoms outnumber the minority ones, resulting in high magnetic moment for the three nanowires. More specifically, for the $[V(FeCp_2)]_\infty$ nanowire, its magnetic moment stems mainly from dσ and dδ electrons of V atoms and dπ electrons of Fe atoms. For $[Ti(FeCp_2)]_\infty$, most of the d-DOS of Fe atoms disperses over the range of -3 to -0.5 eV (dσ and dδ) while that of Ti atom is just below the Fermi level. The magnetism of $[Ti(FeCp_2)]_\infty$, mainly arises from dσ and dπ electrons of Ti and Fe atoms. For $[Mn(FeCp_2)]_\infty$, however, d electrons of Mn almost equally distribute in the majority and minority channels. Magnetism of $[Mn(FeCp_2)]_\infty$ is due mainly to dπ and dδ electrons of Fe atoms. For $[Sc(FeCp_2)]_\infty$, little exchange splitting occurs and unpaired electrons in the dδ orbitals of Sc near the Fermi level dominate nanowire's magnetic behavior.

The different magnetic behavior among $[TM(FeCp_2)]_\infty$ sandwich nanowires can be further understood from their difference in the electron filling, as shown for finite-size clusters. Taking $[V(FeCp_2)]_\infty$ as an example, below the Fermi level, eight d orbitals of Fe atoms and three d orbitals of V atom can be identified, indicating that two valence electrons of V atom are transferred to its neighboring Cp rings. Thus, the V and Fe atoms have three and two unpaired electrons, consistent with calculated Mulliken spin of 3.097 and 2.125 μ_B, respectively. Likewise, in $V_3(FeCp_2)_4$, the center V atom transfers two electrons to its side Cp rings and contributes a local magnetic moment of 3 μ_B.

CONCLUSION

Structural, electronic, and magnetic properties of multidecker sandwich clusters $TM_n(FeCp_2)_{n+1}$ [TM = V, Ti, Sc, Mn, n = 1–3] and 1D $[TM(FeCp_2)]_\infty$ sandwich nanowires have been studied by using gradient-corrected density functional theory. The $TM_n(FeCp_2)_{n+1}$ clusters are highly stable and form polyferrocene-like sandwich structures because of strong Fe–Cp interaction. The $Mn_n(FeCp_2)_{n+1}$ clusters have stronger Fe–Cp and weaker Mn–Cp interaction than the other three systems. The total magnetic moment of $TM_n(FeCp_2)_{n+1}$ (TM = V, Ti, Mn) increases linearly with the size n. More strikingly, $Ti_n(FeCp_2)_{n+1}$ and $V_n(FeCp_2)_{n+1}$ exhibit giant magnetic moments 4, 8, 12 μ_B and 1, 6, 11 μ_B, respectively for n = 1–3.

$[TM(FeCp_2)]_\infty$ sandwich nanowires also show distinctive magnetic properties. All the four nanowires are ferromagnetic semiconductors. A relatively large band gap of 1.310 eV is found for $[Mn(FeCp_2)]_\infty$ among the four, while $[V(FeCp_2)]_\infty$ nanowire possesses the highest magnetic moment (5 μ_B) per unit cell. The tunable magnetic properties of TM–Cp sandwich clusters and nanowires may be exploited for applications in nanoelectronics and spintronics.

COMPUTATIONAL METHODS

We used density functional theory (DFT) methods with the Perdew–Wang gradient-corrected functional (PW91)[63] and all-electron double numerical basis set with polarization functions (DNP basis set) implemented in the DMol3 package.[64] A convergence criterion of 10^{-6} au on total energy and electron density was adopted for the self-consistent field calculations. The global cutoff was set to 5.5 Å. Geometry optimization was performed using the Broyden–Fletcher–Goldfarb–Shanno algorithm with a convergence criterion of 10^{-3} au on the displacement and the gradient and 10^{-5} au on the total energy. Reliability of the PW91/DNP level of theory was tested through a series of calculations for single Sc, Ti, V, and Mn atoms, a ferrocene complex, as well as corresponding metallocenes. As shown in Table 3, the PW91/DNP level of theory reproduces experimental values of ionization energy of Sc, Ti, V, Mn atom, C–C, and C–H bond lengths, metal–ligand distances, binding energy and ionization energy of metallocene molecules.[57,65,66]

All multidecker sandwich clusters whose initial structure has D_{5h} symmetry were fully optimized without any symmetry constraint. During the optimization, a cluster's spin state was determined by checking the "auto" set in the DMol3 package. Next, to ensure the cluster was not trapped in a local-minimum spin state, various spin projection values were assigned to the cluster; geometry optimization was then reperformed for each given spin state. The lowest-energy structures were further verified to be true minima via harmonic frequency computation using the DFT-based semicore pseudopotential basis set (DSPP) implemented in DMol^3 package.

For $[TM(FeCp_2)]_\infty$ sandwich nanowires, the unit cell consists of a FeCp$_2$ molecule and a TM atom, as shown in Figure 1. Periodic boundary conditions were applied along the nanowire direction (z direction). The lattice constant c (in z direction) is equal to the sum of the distance between the TM atom and their adjacent C$_5$H$_5$ ring or the distance between two C$_5$H$_5$ rings in FeCp$_2$ molecule. The lattice parameters in x and y directions are fixed at 15 Å to ensure interaction between the nanowire and its image negligible. Structural optimization was taken with the Monk-

TABLE 3. Comparison of DFT Results (PW91/DNP) with Experimental (exptl) Ones for Benchmark Systems: Fe, V, Ti, Sc, Mn, MnCp$_2$, FeCp$_2$, and VCp$_2$. R_{TM-Cp} is the Distance between Transition Metal Atom and the Mass Center of the C$_5$H$_5$ Ligand. IP is the Ionization Potential

system	properties	theory	exptl
Fe	IP (eV)	7.72	7.7~7.92[a]
Sc	IP (eV)	5.795	6.54—6.70[a]
Ti	IP (eV)	6.351	6.01—7.30[a]
V	IP (eV)	7.050	6.74~7.50[a]
Mn	IP (eV)	7.22	7.430~7.435[a]
MnCp$_2$	R_{C-C} (Å)	1.429	1.429 ± 0.008[b]
	R_{C-H} (Å)	1.086	1.125 ± 0.010[b]
	R_{TM-Cp} (Å)	2.113	2.046 ± 0.008[b]
	IP (eV)	6.645	6.18~7.30[a]
FeCp$_2$	R_{C-C} (Å)	1.432	1.440 ± 0.002[b]
	R_{C-H} (Å)	1.086	1.104 ± 0.006[b]
	R_{TM-Cp} (Å)	1.670	1.660[b]
	IP (eV)	6.951	6.60~7.20[a]
	E_b (eV)	8.22	6.938[c]
VCp$_2$	R_{C-C} (Å)	1.425	1.434 ± 0.003[b]
	R_{C-H} (Å)	1.087	1.133 ± 0.014[b]
	R_{TM-Cp} (Å)	1.942	1.928 ± 0.006[b]
	IP (eV)	6.78	6.78, 6.70—7.30[a]

[a]Reference 65. [b]Reference 57. [c]Reference 66.

horst-Pack grid of 1 × 1 × 12-points sampling without symmetry constraint. Electronic density of state (DOS) was calculated with 24 k points sampling in the 1D Brillouin zone.

Supporting Information Available: Geometric structures of the lowest-energy multidecker sandwich clusters TM$_n$(FeCp$_2$)$_{n+1}$ are shown in Figure S1. This material is available free of charge *via* the Internet at http://pubs.acs.org.

REFERENCES AND NOTES

1. Kealy, T. J.; Pauson, P. L. A New Type of Organo-Iron Compound. *Nature* **1951**, *168*, 1039–1040.
2. Long, N. J. *In Metallocenes: An Introduction to Sandwich Complexes*, Blackwell Science: Oxford, U.K. 1998.
3. Weis, P.; Kemper, P. R.; Bowers, M. T. Structures and Energetics of V$_n$(C$_6$H$_6$)$_m^+$ Clusters: Evidence for a Quintuple-Decker Sandwich. *J. Phys. Chem. A* **1997**, *101*, 8207–8213.
4. Kurikawa, T.; Takeda, H.; Hirano, M.; Judai, K.; Arita, T.; Nagao, S.; Nakajima, A.; Kaya, K. Electronic Properties of Organometallic Metal-Benzene Complexes [M$_n$(benzene)$_m$ (M = Sc—Cu)]. *Organometallics* **1999**, *18*, 1430–1438.
5. Nakajima, A.; Kaya, K. A Novel Network Structure of Organometallic Clusters in the Gas Phase. *J. Phys. Chem. A* **2000**, *104*, 176–191.
6. Hoshino, K.; Kurikawa, T.; Takeda, H.; Nakajima, A.; Kaya, K. Structures and Ionization Energies of Sandwich Clusters (V$_n$(Benzene)$_m$). *J. Phys. Chem.* **1995**, *99*, 3053–3055.
7. Miyajima, K.; Nakajima, A.; Yabushita, S.; Knickelbein, M. B.; Kaya, K. Ferromagnetism in One-Dimensional Vanadium-Benzene Sandwich Clusters. *J. Am. Chem. Soc.* **2004**, *126*, 13202–13203.
8. Miyajima, K.; Yabushita, S.; Knickelbein, M. B.; Nakajima, A. Stern—Gerlach Experiments of One-Dimensional Metal—Benzene Sandwich Clusters: M$_n$(C$_6$H$_6$)$_m$ (M = Al, Sc, Ti, and V). *J. Am. Chem. Soc.* **2007**, *129*, 8473–8480.
9. Pandey, R.; Rao, B. K.; Jena, P.; Newsam, J. M. Unique Magnetic Signature of Transition Metal Atoms Supported on Benzene. *Chem. Phys. Lett.* **2000**, *321*, 142–150.
10. Pandey, R.; Rao, B. K.; Jena, P.; Blanco, M. A. Electronic Structure and Properties of Transition Metal—Benzene Complexes. *J. Am. Chem. Soc.* **2001**, *123*, 3799–3808.
11. Kandalam, A. K.; Rao, B. K.; Jena, P.; Pandey, R. Organometallic Benzene—Vanadium Wire: A One-Dimensional Half-Metallic Ferromagnet. *J. Chem. Phys.* **2004**, *120*, 10414.
12. Wang, J.; Acioli, P. H.; Jellinek, J. Structure and Magnetism of V$_n$Bz$_{n+1}$ Sandwich Clusters. *J. Am. Chem. Soc.* **2005**, *127*, 2812–2813.
13. Wang, J.; Jellinek, J. Infrared Spectra of V$_n$Bz$_{n+1}$ Sandwich Clusters: A Theoretical Study of Size Evolution. *J. Phys. Chem. A* **2005**, *109*, 10180–10182.
14. Zheng, W. J.; Nilles, J. M.; Thomas, O. C.; Bowen, K. H., Jr. Photoelectron Spectroscopy of Titanium—Benzene Cluster Anions. *Chem. Phys. Lett.* **2005**, *401*, 266–270.
15. Kua, J.; Tomlin, K. M. Computational Study of Multiple-Decker Sandwich and Rice-Ball Structures of Neutral Titanium—Benzene Clusters. *J. Phys. Chem. A* **2006**, *110*, 11988–11994.
16. Rahman, M. M.; Kasai, H.; Dy, E. S. Theoretical Investigation of Electric and Magnetic Properties of Benzene—Vanadium Sandwich Complex Chain. *Jpn. J. Appl. Phys.* **2005**, *44*, 7954–7956.
17. Xiang, H. J.; Yang, J. L.; Hou, J. G.; Zhu, Q. S. One-Dimensional Transition Metal—Benzene Sandwich Polymers: Possible Ideal Conductors for Spin Transport. *J. Am. Chem. Soc.* **2006**, *128*, 2310–2314.
18. Maslyuk, V. V.; Bagrets, A.; Meded, V.; Arnold, A.; Evers, F.; Brandbyge, M.; Bredow, T.; Mertig, I. Organometallic Benzene—Vanadium Wire: A One-Dimensional Half-Metallic Ferromagnet. *Phys. Rev. Lett.* **2006**, *97*, 097201.
19. Mokrousov, Y.; Atodiresei, N.; Bihlmayer, G.; Gel, S. Magnetic Anisotropy Energies of Metal-Benzene Sandwiches. *Int. J. Quantum Chem.* **2006**, *106*, 3208–3213.
20. Mokrousov, Y.; Atodiresei, N.; Bihlmayer, G.; Gel, S.; Blugel, S. The Interplay of Structure and Spin—Orbit Strength in the Magnetism of Metal—Benzene Sandwiches: From Single Molecules to Infinite Wires. *Nanotechnology* **2007**, *18*, 495402.
21. Weng, H. M.; Ozaki, T.; Terakura, K. Theoretical Analysis of Magnetic Coupling in Sandwich Clusters V$_n$(C$_6$H$_6$)$_{n+1}$. *J. Phys. Soc. Jpn.* **2008**, *77*, 014301.
22. Kurikawa, T.; Negishi, Y.; Satoshi, F. H.; Nagao, S.; Miyajima, K.; Nakajima, A.; Kaya, K. Multiple-Decker Sandwich Complexes of Lanthanide-1,3,5,7-Cyclooctatetraene [Ln$_n$(C$_8$H$_8$)$_m$] (Ln = Ce, Nd, Eu, Ho, and Yb); Localized Ionic Bonding Structure. *J. Am. Chem. Soc.* **1998**, *120*, 11766–11772.
23. Liu, W. J.; Dolg, M.; Fulde, P. Calculated Properties of Lanthanocene Anions and the Unusual Electronic Structure of Their Neutral Counterparts. *Inorg. Chem.* **1998**, *37*, 1067–1072.
24. Li, J.; Bursten, E. Relativistic Density Functional Study of the Geometry, Electronic Transitions, Ionization Energies, and Vibrational Frequencies of Protactinocene, Pa(η^8-C$_8$H$_8$)$_2$. *J. Am. Chem. Soc.* **1998**, *120*, 11456–11466.
25. Miyajima, K.; Knickelbein, M. B.; Nakajima, A. Magnetic Properties of Lanthanide Organometallic Sandwich Complexes Produced in a Molecular Beam. *Polyhedron* **2005**, *24*, 2341–2345.

26. Miyajima, K.; Knickelbein, M. B.; Nakajima, A. Stern−Gerlach Study of Multidecker Lanthanide−Cyclooctatetraene Sandwich Clusters. *J. Phys. Chem. A* **2008**, *112*, 366−375.

27. Scott, A. C.; Foster, N. R.; Grieves, G. A.; Duncan, M. A. Photodissociation of Lanthanide Metal Cation Complexes with Cyclooctatetraene. *Int. J. Mass. Spec.* **2007**, *263*, 171−178.

28. Takegami, R.; Hosoya, N.; Suzumura, J.; Nakajima, A.; Yabushita, S. Geometric and Electronic Structures of Multiple-Decker One-End Open Sandwich Clusters: $Eu_n(C_8H_8)_n^-$ ($n = 1-4$). *J. Phys. Chem. A* **2005**, *109*, 2476−2486.

29. Takegami, R.; Hosoya, N.; Suzumura, J.; Yada, k.; Nakajima, A.; Yabushita, A. Ionization Energies and Electron Distributions of One-End Open Sandwich Clusters: $Eu_n(C_8H_8)_n$ ($n = 1-4$). *Chem. Phys. Lett.* **2005**, *403*, 169−174.

30. Hosoya, N.; Takegami, R.; Suzumura, J.; Yada, K.; Koyasu, K.; Miyajima, K.; Mitsul, M.; Knickelbein, M. B.; Yabushita, S.; Nakajima, A. Lanthanide Organometallic Sandwich Nanowires: Formation Mechanism. *J. Phys. Chem. A* **2005**, *109*, 9−12.

31. Zhou, L.; Yang, S.; Ng, M.; Sullivan, M. B.; Tan, V. B. C.; Shen, L. One-Dimensional Iron−Cyclopentadienyl Sandwich Molecular Wire with Half Metallic, Negative Differential Resistance and High-Spin Filter Efficiency Properties. *J. Am. Chem. Soc.* **2008**, *130*, 4023−4027.

32. Shen, L.; Yang, S.-W.; Ng, M.-F.; Ligatchev, V.; Zhou, L.; Feng, Y. Charge-Transfer-Based Mechanism for Half-Metallicity and Ferromagnetism in One-Dimensional Orgranometallic Sandwich Molecular Wires. *J. Am. Chem. Soc.* **2008**, *130*, 13956−13960.

33. Wang, L; Cai, Z.; Wang, J.; Lu, J.; Luo, G.; Lai, L.; Zhou, J.; Qin, R.; Gao, Z.; Yu, D.; *et al*. Novel One-dimensional Organometallic Half Metals: Vanadium-Cyclopentadienyl, Benzene, and Vanadium Anthracene Wires. *Nano Lett.* **2008**, *8*, 3640−3644.

34. Koleini, M.; Paulsson, M.; Brandbyge, M. Efficient Organometallic Spin Filter between Single-Wall Carbon Nanotube or Graphene Electrodes. *Phys. Rev. Lett.* **2006**, *98*, 197202.

35. Atodiresei, N.; Dederichs, P. H.; Mokrousov, Y.; Bergqvist, L.; Bihlmayer, G.; Blügel, S. Controlling the Magnetization Direction in Molecules *via* Their Oxidation State. *Phys. Rev. Lett.* **2008**, *100*, 117207.

36. Hedberg, L.; Hedberg, K. Molecular Structure of Dicyclopentadienylnickel $(C_5H_5)_2Ni$. *J. Chem. Phys.* **1970**, *53*, 1228.

37. Gard, E.; Haaland, A.; Novak, D. P.; Seip, R. The Molecular Structures of Dicyclopentadienylvanadium, $(C_5H_5)_2V$, and Dicyclopentadienylchromium, $(C_5H_5)_2Cr$, Determined by Gas Phase Electron Diffraction. *J. Organomet. Chem.* **1975**, *88*, 181−189.

38. Hedberg, A. K.; Hedberg, L.; Hedberg, K. Molecular Structure of Di-π-Cyclopentadienylcobalt, $(C_5H_5)_2Co$, by Gaseous Electron Diffraction. *J. Chem. Phys.* **1975**, *63*, 1262.

39. Almenningen, A.; Gard, E.; Haaland, A. Dynamic Jahn−Teller Effect and Average Structure of Dicyclopentadienylcobalt, $(C_5H_5)_2Co$, Studied by Gas Phase Electron Diffraction. *J. Organomet. Chem.* **1976**, *107*, 273−279.

40. Haaland, A. The Molecular Structure of High-Spin Manganocene, $(n-C5H5)2Mn$, by Gas Phase Electron Diffraction: A Rerefinement. *Inorg. Nucl. Chem. Lett.* **1979**, *15*, 267−270.

41. Chhor, K.; Lucazeau, G. Vibrational Study of the Dynamic Disorder in Nickelocene and Ferrocene Crystals. *J. Raman Spectrosc.* **1981**, *11*, 183−198.

42. Almlof, J.; Faegri, K.; Schilling, B. E. R.; Luthi, H. P. Ionization Energies and Electron Distributions of One-End Open Sandwich Clusters: $Eu_n(C_8H_8)_n$ ($n = 1-4$). *Chem. Phys. Lett.* **1984**, *106*, 266−270.

43. Roginski, R. T.; Moroz, A.; Hendrickson, D. N.; Drickamer, H. G. Pressure Tuning of the Electronic Energy Levels of Ferrocene, Cobaltocenium Hexafluorophosphate, and Nickelocene. *J. Phys. Chem.* **1988**, *92*, 4319−4323.

44. Lüthi, H. P.; Ammeter, J. H. How Well Does the Hartree−Fock Model Predict Equilibrium Geometries of Transition Metal Complexes? Large-Scale LCAO−SCF Studies on Ferrocene and Decamethylferrocene. *J. Chem. Phys.* **1982**, *77*, 2002.

45. Michael, R. P.; Yoshiyuki, K. The Electronic Structure of the Dizincocene Core. *Chem. Phys.* **2006**, *327*, 283−290.

46. Shustorovitch, E. M.; Dyatkina, M. E. *Dokl. Akad. Nauk. USSR* **1959**, *123*, 1234. Shustorovitch, E. M.; Dyatkina, M. E. The Molecular Orbital Self-Consistent-Field Determination of the Ground State of Ferrocene. *J. Struct. Chem. (USSR)* **1960**, *1*, 98−110.

47. Aleksanyan, V. T.; Greenwald, I. I. Investigation of Charge Separation in Dicyclopentadienyl Complexes of Metals by Theoretical Analysis of Infrared Intensities. *J. Mol. Struct. (THEOCHEM)* **1982**, *90*, 35−47.

48. Weber, J.; Goursot, A.; Penigault, E.; Ammeter, J. H.; Bachmann, J. Electronic Structure of Metallocene Compounds. 3. Comparison of the Results of Multiple-Scattering X.Alpha. Calculations with Various Electronic Observables of Cobaltocene. *J. Am. Chem. Soc.* **1982**, *104*, 1491−1506.

49. Rosch, N.; Jorg, H. A Linear Combination of Gaussian-Type Orbitals (LCGTO) $X\alpha$ Study of Ferrocene: The Metal-to-Ring Distance and Ionization Potentials. *J. Chem. Phys.* **1986**, *84*, 5967.

50. Park, C.; Almlof, J. The Electronic and Molecular Structure of Ferrocene. *J. Chem. Phys.* **1991**, *95*, 1829.

51. Pierloot, K.; Persson, B. J.; Roos, B. O. Theoretical Study of the Chemical Bonding in $[Ni(C_2H_4)]$ and Ferrocene. *J. Phys. Chem.* **1995**, *99*, 3465−3472.

52. Koch, H.; Jorgensen, P.; Helgaker, T. The Molecular Structure of Ferrocene. *J. Chem. Phys.* **1996**, *104*, 9528.

53. Berces, A.; Ziegler, T.; Fan, L. Density Functional Study of the Harmonic Force Fields of Cyclopentadienyl Anion, Cyclopentadienyl Lithium, and Ferrocene. *J. Phys. Chem.* **1994**, *98*, 1584−1595.

54. Mayor-Lopez, M. J.; Weber, J. DFT Calculations of the Binding Energy of Metallocenes. *Chem. Phys. Lett.* **1997**, *281*, 226−232.

55. Matsuzawa, N.; Seto, J. Density Functional Theory Predictions of Second-Order Hyperpolarizabilities of Metallocenes. *J. Phys. Chem. A* **1997**, *101*, 9391−9398.

56. Schreckenbach, G. The ^{57}Fe Nuclear Magnetic Resonance Shielding in Ferrocene Revisited. A Density-Functional Study of Orbital Energies, Shielding Mechanisms, and the Influence of the Exchange-Correlation Functional. *J. Chem. Phys.* **1999**, *110*, 11936.

57. Xu, Z. F.; Xie, Y. M.; Feng, W. L.; Schaefer, H. F. Systematic Investigation of Electronic and Molecular Structures for the First Transition Metal Series Metallocenes $M(C_5H_5)_2$ (M = V, Cr, Mn, Fe, Co, and Ni). *J. Phys. Chem. A* **2003**, *107*, 2716−2729.

58. Salter, A.; Warner, H. A New Route to Triple-Decker Sandwich Compounds. *Angew. Chem., Int. Ed. Engl.* **1972**, *11*, 930.

59. Schilderout, S. M. High-Pressure Mass Spectra and Gaseous Ion Chemistry of Ferrocene. *J. Am. Chem. Soc.* **1973**, *95*, 3846−3849.

60. Nagao, S.; Kato, A.; Nakajima, A. Multiple-Decker Sandwich Poly-Ferrocene Clusters. *J. Am. Chem. Soc.* **2000**, *122*, 4221−4222.

61. Frisch, M. J.; Trucks, G. W.; Schlegel, H. B.; Scuseria, G. E.; Robb, M. A.; Cheeseman, J. R.; Montgomery, J. A., Jr.; Vreven, T.; Kudin, K. N.; Burant, J. C.; *et al. Gaussian 03*, revision C.02; Gaussian, Inc.: Wallingford, CT, 2004.

62. Mallajosyula, S. S.; Pati, S. K. Vanadium-Benzimidazole-Modified sDNA: A One-Dimensional Half-Metallic Ferromagnet. *J. Phys. Chem. B* **2007**, *111*, 13877−13880.

63. Perdew, J. P.; Wang, Y. Accurate and Simple Analytic Representation of the Electron-Gas Correlation Energy. *Phys. Rev. B* **1992**, *45*, 13244.
64. *DMOL, Density Functional Theory Program*; Accelrys, Inc.: San Diego, CA. Delley, B. An All-Electron Numerical Method for Solving the Local Density Functional for Polyatomic Molecules. *J. Chem. Phys.* **1990**, *92*, 508. From Molecules to Solids with the DMol³ Approach. *J. Chem. Phys.* **2000**, *113*, 7756.
65. NIST Standard Reference Database 69-March 2003 Release: NIST Chemistry WebBook; http://webbook.nist.gov.
66. Richardson, D. E.; Christ, C. S.; Sharpe, P.; Ryan, M. F.; Eyler, J. R. In *Bond Energetics in Organometallic Compounds*; Marks, T., Ed.; ACS Symposium Series 428; American Chemical Society: Washington, DC, 1990.